DNA coated CoZn-ZIF metal-organic frameworks for fluorescent sensing guanosine triphosphate and discrimination of nucleoside triphosphates

Zhen Wang[1,2], Xumei Zhou[1], Jing Han[1], Gang Xie[1*] and Juewen Liu[2*]

[1]Key Laboratory of Synthetic and Natural Functional Molecule Chemistry of Ministry of Education, College of Chemistry & Materials Science, Northwest University, Xi'an, Shaanxi 710127, China
Email: xiegang@nwu.edu.cn

[2]Department of Chemistry, Waterloo Institute for Nanotechnology, University of Waterloo, Waterloo, Ontario N2L 3G1, Canada
Email: liujw@uwaterloo.ca

ABSTRACT

Imidazole-based metal-organic frameworks (MOFs) are easy to prepare as well-dispersed nanoparticles, which have attracted a lot of interest in cation/anion sensing. Metal substitution is an effective way to regulate the composition and performance of MOFs. Herein, by tuning the contents of Co and Zn, a series of homobimetallic Co_xZn_{100-x}-ZIF (x=0-100) were synthesized. Using a fluorescently-labeled DNA oligonucleotide probe, guanosine triphosphate (GTP) can readily displace the adsorbed DNA from $Co_{50}Zn_{50}$-ZIF, resulting in over 30-fold fluorescence enhancement with 1 mM GTP. $Co_{80}Zn_{20}$-ZIF could specifically recognize adenosine triphosphate (ATP), whereas $Co_{65}Zn_{35}$-ZIF and $Co_{20}Zn_{80}$-ZIF responded to both. For comparison, $Co_{50}Ni_{50}$-ZIF and $Co_{50}Cu_{50}$-ZIF were also prepared, but none of them were selective for any of the molecules, indicating a synergetic effect of cobalt and zinc in $Co_{50}Zn_{50}$-ZIF for the selective recognition of GTP. This system can sensitively detect GTP with a detection limit of 0.13 μM. Moreover, based on the varying binding affinities of these CoZn-ZIFs towards different nucleoside triphosphates (NTPs), a ZIF fluorescent sensor array was also designed for the discrimination of the four types of NTPs.

Keywords: biosensors; MOF; DNA; fluorescence; GTP; nucleotides

1. Introduction

Guanosine triphosphate (GTP) is a vital nucleotide that regulates numerous cellular processes [1], [2], [3]. It is also a substrate for the synthesis of RNA [4], and serves as an energy source for some metabolic reactions and protein synthesis [5,6]. The concentration of GTP is closely related to pathological states and is a chemical indicator of a variety of human diseases [7,8]. Consequently, selective detection of GTP is of analytical importance. To date, considerable efforts have been devoted for GTP detection including using high performance liquid chromatography (HPLC) [9,10], mass spectrometry [11], electrochemistry [12], colorimetry and fluorescence [13,14]. However, some of them suffer from expensive equipment and multistep and time-consuming procedures. Assays based on organic GTP probes usually require sophisticated synthesis and purification [15], [16], [17]. Furthermore, many GTP biosensors are not selective enough and can also respond to other phosphate-containing species, such as orthophosphate, pyrophosphate and other nucleoside triphosphates due to their similar structures and binding modes [18], [19], [20]. Accordingly, it is essential to develop a simple, selective, and sensitive biosensor for GTP detection.

Instead of using biomolecules for sensing GTP, molecular recognition by nanomaterials provides an alternative way for sensing [21]. For example, metal-organic frameworks (MOFs) have attracted great interest in sensing due to their adjustable structures and functions [22,23]. The detected analytes include ammonia [24], metal ions [25,26], and toxic gases [27], [28], [29]. We recently discovered that a classic Co-based MOF material, ZIF-67 (zeolite imidazole framework-67) exhibited ultrahigh selectivity for the detection of adenosine triphosphate (ATP), and its specificity was even better than the ATP aptamer [30,31]. When replacing Co^{2+} by Zn^{2+} to form ZIF-8, the selectivity for ATP was lost, and ZIF-8 responded nonspecifically to all phosphate containing molecules.

Metal substitution is an efficient way to modulate the composition of ZIFs [32,33]. By partially replacing Zn^{2+} with other transition metals in ZIF-8 to form various bimetallic M/Zn-ZIFs (M=Ni, Mn, Cu), we found that Cu/ZIF-8 showed an excellent selectivity for pyrophosphate (PPi) [34]. However, the doping efficiency of most secondary metal ions was quite low [35,36]. When 50% Cu^{2+} was doped, the ZIF-8 framework completely collapsed [37]. The ionic radii of Co^{2+} (0.72 Å) and Zn^{2+} (0.74 Å) are comparable [38]. In addition, zeolitic ZIF-67 (Co^{2+} based) and ZIF-8 (Zn^{2+} based) are isostructural, which may allow more flexibility in metal mixing. CoZn-ZIFs were used in gas adsorption, catalysis [39,40], and templated synthesis [[41], [42], [43]].

Herein, we synthesized a series of homobimetallic Co_xZn_{100-x}-ZIF (x=0-100) with varying Co contents. Using a fluorescently labeled single-stranded DNA (ssDNA) as a signaling probe, DNA adsorption on these CoZn-ZIFs and desorption induced by GTP and other nucleotides was further performed. DNA was used since it is a polymer of nucleotides and can be a good competitor for the detection of GTP. Interestingly, $Co_{50}Zn_{50}$-ZIF exhibited excellent selectivity for GTP, $Co_{80}Zn_{20}$-ZIF could specifically recognize ATP, whereas $Co_{65}Zn_{35}$-ZIF and $Co_{20}Zn_{80}$-ZIF responded to both. Based on the varying binding affinities of these CoZn-ZIFs towards different nucleoside triphosphates (NTPs), a highly sensitive ZIF fluorescent sensor array was designed for the discrimination of NTPs.

2. Experimental section

2.1. Chemicals

Zinc nitrate ($Zn(NO_3)_2$), cobalt(II) nitrate ($Co(NO_3)_2$), 2-methylimidazole (2-MI), copper chloride ($CuCl_2$), nickel chloride ($NiCl_2$), sodium pyrophosphate (PPi), adenosine monophosphate (AMP), guanosine monophosphate (GMP), cytidine monophosphate (CMP), adenosine triphosphate (ATP), guanosine triphosphate (GTP), cytidine triphosphate (CTP), uridine triphosphate (UTP), sodium triphosphate (STPP), bovine serum albumin (BSA) and fetal bovine serum (FBS) were purchased from Sigma-Aldrich. (St. Louis, USA), and all of the chemical reagents are analytical reagent (A.R.) grade. 4-(2-Hydroxyethyl) piperazine-1-ethane sulfonate (HEPES) and the four ribonucleosides were purchased from Mandel Scientific (Guelph, Ontario, Canada). Milli-Q water was used for preparing the buffers and solutions. All the DNA samples were purchased from Integrated DNA Technologies (IDT, Coralville, IA, USA), and their sequences are:

FAM-12mer: 5′-FAM-AGAGAACCTGGG-3′

Random DNA (rDNA): 5′-TCACAGATGCGT-3′

2.2. Instrumentation and characterization

Zeta-potential was measured using dynamic light scattering (DLS, Zetasizer Nano 90, Malvern) in HEPES buffer (10 mM, pH 7.6). The morphologies and structural analysis of different ZIFs were carried out by scanning electron microscopy (SEM, Carl Zeiss), transmission electron microscopy (TEM, Talos-F200X) and powder X-ray diffraction (PXRD, Bruker D8). The amount of the actual metal ions (Co, Zn, Ni and Cu) in different ZIF samples was measured using inductively-coupled plasma mass spectrometry (ICP-MS, Agilent 7900). The fluorescent intensity was recorded on a microplate reader (Infinite F200 Pro, Tecan) with

485 nm excitation and 535 nm emission.

2.3. Synthesis of bimetallic CoM-ZIFs (M = Zn, Ni, Cu)

A series of bimetallic CoZn-ZIFs labeled as Co_xZn_{100-x}-ZIF (x= 0-100) were prepared following the previous literature with slight modification [44]. In brief, $Co(NO_3)_2$ and/or $Zn(NO_3)_2$ were first dissolved in 7 mL methanol, and the total molar amount of Zn and Co was fixed at 0.5 mmol. Then 4 mmol 2-MI dissolved in 7 mL methanol was rapidly added into the above solution and kept static for 24 h at room temperature. The molar percentages of $Co(NO_3)_2$ used was 100%, 80%, 65%, 50%, 20% and 0% to obtain ZIF-67 (Co), $Co_{80}Zn_{20}$-ZIF, $Co_{65}Zn_{35}$-ZIF, $Co_{50}Zn_{50}$-ZIF, $Co_{20}Zn_{80}$-ZIF, and ZIF-8 (Zn), respectively. Finally, the products were separated by centrifugation, washed with methanol and then dried overnight at 60 °C. $Co_{50}Ni_{50}$-ZIF and $Co_{50}Cu_{50}$-ZIF were also prepared using the method similar to $Co_{50}Zn_{50}$-ZIF, except that Zn^{2+} was replaced by Ni^{2+} or Cu^{2+}.

2.4. DNA adsorption on bimetallic CoZn-ZIFs

Typically, different CoZn-ZIFs (100 μg/mL) were respectively incubated with FAM-12mer (10 nM) in HEPES buffer (10 mM, pH 7.6) for 40 min. After centrifugation, the microplate reader was used to record the fluorescence intensity of the unadsorbed DNA in the supernatant.

2.5. DNA desorption

To study DNA desorption, pre-adsorbed FAM-12mer/CoZn-ZIF complexes were first dispersed in HEPES buffer (10 mM, pH 7.6) with quenched fluorescence. After the addition of different competing molecules and incubation for another 55 min, the samples were centrifuged and the fluorescence recovery of the supernatant indicating the amount of desorbed DNA was measured.

2.6. Determination of GTP

To detect GTP, 10 nM FAM-12mer was first adsorbed on 100 μg/mL $Co_{50}Zn_{50}$-ZIF in HEPES buffer (10 mM, pH 7.6). Afterwards, GTP of different concentrations was added into the FAM-12mer/$Co_{50}Zn_{50}$-ZIF dispersion. DNA desorption was followed by monitoring the kinetics of fluorescence increase. Then the fold of fluorescence enhancement (F/F_0-1) was calculated to compare the fluorescence recovery, where F_0 and F represent the fluorescence intensity of the sample in the absence and presence of GTP, respectively.

2.7. Discrimination of different NTPs by a CoZn-ZIF sensor array

To evaluate the discrimination capability of the CoZn-ZIF sensor array toward the four types of NTPs, FAM-12mer (10 nM) was first respectively adsorbed on 100 μg/mL $Co_{80}Zn_{20}$-ZIF, $Co_{65}Zn_{35}$-ZIF, $Co_{50}Zn_{50}$-ZIF and $Co_{20}Zn_{80}$-ZIF in HEPES buffer (10 mM, pH 7.6). Then the DNA fluorescence recovery induced by ATP, GTP, CTP and UTP were respectively recorded, and fluorescence enhancement (F/F_0-1) was calculated. The experiment was repeated six times. Finally, the OriginLab software was used to perform principal component analysis (PCA) and hierarchical cluster analysis (HCA) on the basis of fluorescence pattern of the training matrix (4 ZIFs × 4 NTPs × 6 replicates).

2.8. GTP assay in diluted serum

To further test the practicality of the proposed GTP biosensor, 1% fetal bovine serum (FBS) diluted with 10 mM HEPES (pH 7.6) was used. The pre-adsorbed FAM-12mer/$Co_{50}Zn_{50}$-ZIF complex was first dispersed in FBS. Then different concentrations of GTP were added and the fluorescence enhancements were monitored.

3. Results and discussion

3.1 Synthesis and characterization of bimetallic CoZn-ZIFs

A series of bimetallic Co_xZn_{100-x}-ZIFs (x=0-100) were synthesized *via* a simple co-precipitation method (Figure 1A) by mixing 2-methylimidazole (2-MI) and metal sources (Co^{2+} and Zn^{2+}) with varying molar percentages of Co^{2+} (x=100, 80, 65, 50, 20 and 0) in methanol. The mixtures became cloudy and finally precipitated, and the samples were named ZIF-67 (Co), $Co_{80}Zn_{20}$-ZIF, $Co_{65}Zn_{35}$-ZIF, $Co_{50}Zn_{50}$-ZIF, $Co_{20}Zn_{80}$-ZIF, and ZIF-8 (Zn), respectively.

Incorporation of Zn^{2+} in the ZIF-67 (Co) framework can be observed by a visible color change from violet to white upon increasing the Zn content (the insets in Figure 1, Figure S1). Because the ionic radii of Co^{2+} (0.72 Å) and Zn^{2+} (0.74 Å) are comparable, bimetallic CoZn-ZIFs are expected to be feasible due to the isostructural feature of ZIF-8 ($Zn(Hmim)_2$) and ZIF-67 ($Co(Hmim)_2$). In addition, SEM images from Figure 1B to Figure 1G showed that they were all regular hexagonal nanoparticles with a size distribution in the range of 50 nm to 200 nm. Moreover, with increasing Zn content, nucleation centers increased and the average diameter of the CoZn-ZIFs gradually decreased, which indicated a kinetically controlled growth of the ZIFs [45].

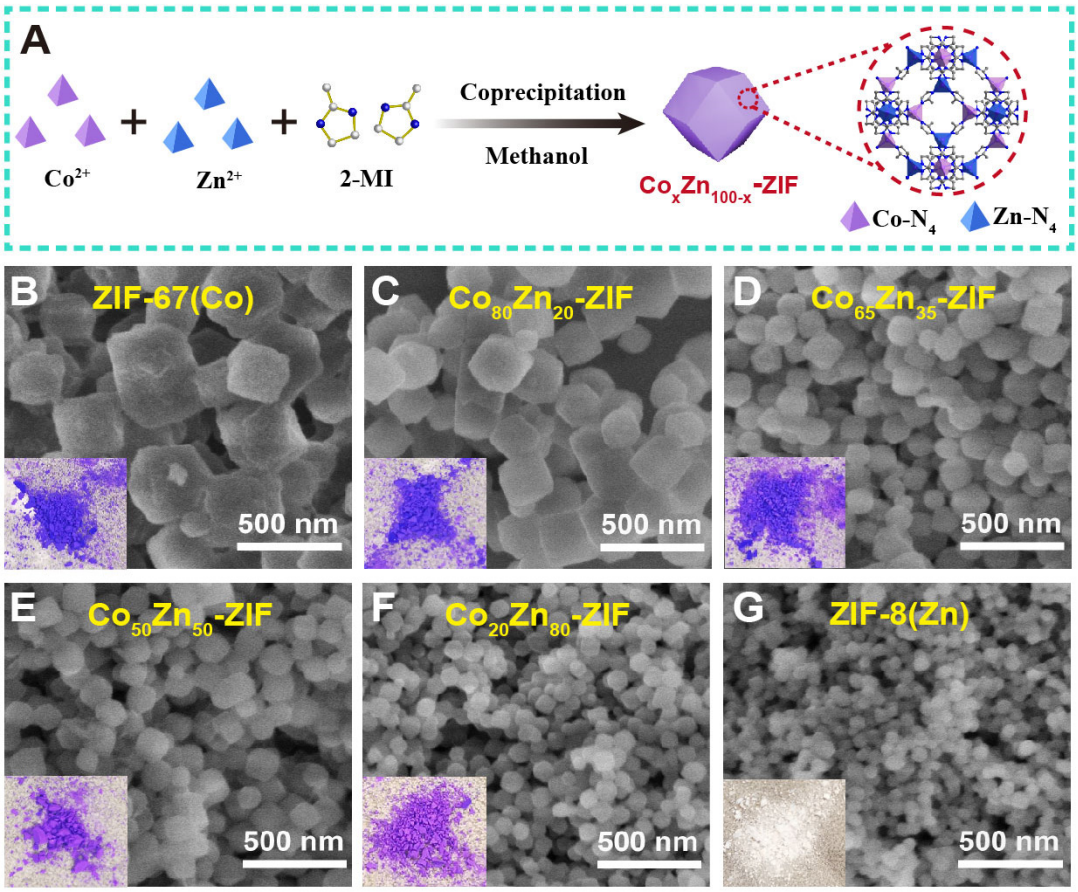


Figure 1. (A) Schematic illustration of co-precipitation synthesis of Co_xZn_{100-x}-ZIF. SEM images of (B) ZIF-67 (Co), (C) $Co_{80}Zn_{20}$-ZIF, (D) $Co_{65}Zn_{35}$-ZIF, (E) $Co_{50}Zn_{50}$-ZIF, (F) $Co_{20}Zn_{80}$-ZIF, and (G) ZIF-8 (Zn). Inset: photographs of the synthesized ZIF samples (the size of these pictures is 1 cm × 1 cm).

Using $Co_{50}Zn_{50}$-ZIF as an example, the TEM image in Figure 2A indicated its regular morphology and size distribution. The high-angle annular dark field scanning TEM (HAADF-STEM) and energy dispersive spectrometry (EDS) elemental mapping in Figure 2B further revealed a homogenously distribution of Co and Zn in $Co_{50}Zn_{50}$-ZIF. ICP-MS was then used to determine the final contents of cobalt and zinc in these bimetallic ZIFs. The actual percentages of Co were within 7% of the initially added content (Table 1), indicating effective co-precipitation of all of the metal ions with 2-MI.

The structures of these CoZn-ZIFs were then verified by powder X-ray diffraction (PXRD) (Figure 2C). They were all in good agreement with the theoretically simulated ZIF structure, especially the very sharp peaks below 10° (with 2θ of 7.3) and above 12° (with 2θ of 12.6°) indicated high crystallinity [46]. Therefore, we have successfully synthesized the six ZIFs. Finally, they were all positively charged in water as judged from the zeta-potentials (Figure 2D), and thus they were expected to adsorb negatively charged DNA [47,48].

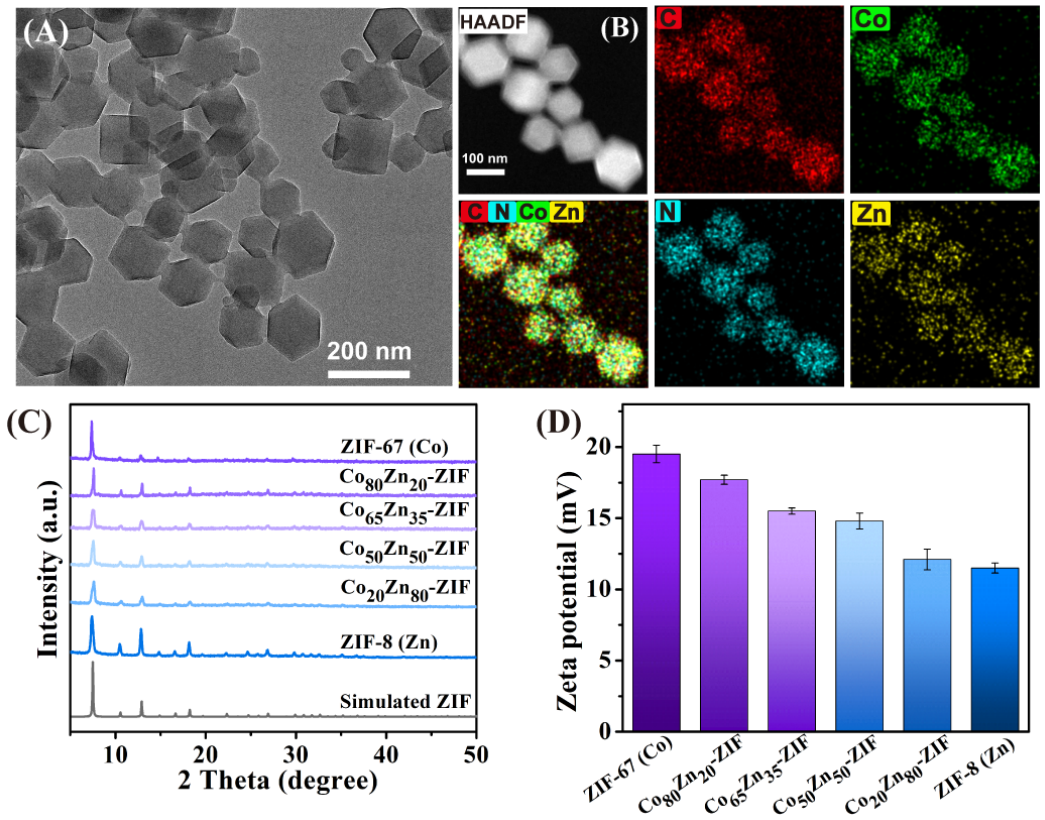


Figure 2. (A) TEM image and (B) HAADF-STEM elemental mapping of $Co_{50}Zn_{50}$-ZIF. (C) PXRD patterns and (D) zeta-potentials measured in HEPES buffer (10 mM, pH 7.6) of the six CoZn-ZIFs. Each measurement was run in triplicate.

Table 1 ICP-MS data for measuring the Co content in different CoZn-ZIF samples in comparison to the initial molar percent during the synthesis.

Sample	2-MI (mmol)	$Co(NO_3)_2$ (mmol)	$Zn(NO_3)_2$ (mmol)	Initial Co content (mol%)	Co content (mol%) from ICP-MS
ZIF-67(Co)	4	0.5	0	100	99.6
$Co_{80}Zn_{20}$-ZIF	4	0.4	0.1	80	84.1
$Co_{65}Zn_{35}$-ZIF	4	0.33	0.17	65	66.8
$Co_{50}Zn_{50}$-ZIF	4	0.25	0.25	50	55.7
$Co_{20}Zn_{80}$-ZIF	4	0.1	0.4	20	26.3
ZIF-8(Zn)	4	0	0.5	0	0.03

3.2 $Co_{50}Zn_{50}$-ZIF is highly selective for GTP

Based on our previous studies [30], both ZIF-67 (Co) and ZIF-8 (Zn) can strongly adsorb fluorophore-labeled DNA and quench the fluorescence emission. Since ZIF-8 (Zn) is stable in

neutral pH but quickly decomposes when suspended in acidic solutions, the optimal pH for our experiments is neutral physiological conditions (HEPES buffer, pH 7.6). In this work, using a FAM (6-carboxyfluorescein)-labeled 12-mer DNA oligonucleotide (named FAM-12mer) as a fluorescence indicator, the interaction between DNA and the four CoZn-ZIFs were investigated. Here, DNA was used only as a signaling probe, and the sequence of DNA is not important as long as the ZIFs can adsorb the DNA. Since DNA has nucleosides and phosphate as building blocks, we used them as competitive molecules to displace the adsorbed DNA, and DNA desorption was accompanied with fluorescence enhancement (Figure 3A) [48,49].

The negatively charged FAM-12mer was first pre-adsorbed on the four positively charged Co_xZn_{100-x}-ZIFs (x= 80, 65, 50 and 20). Then different competing molecules including four kinds of nucleosides (adenosine, thymidine, cytidine, and guanosine) and different phosphate containing competitors such as orthophosphate, pyrophosphate (PPi), triphosphate (STPP), nucleoside mono- and triphosphates were used to desorb the FAM-12mer.

For $Co_{80}Zn_{20}$-ZIF (Figure 3B), ATP gave the highest fluorescence signal and thus the most DNA desorption, GTP showed about 26% DNA desorption, while the other species induced much lower responses. This pattern of response was similar to that from ZIF-67 (Co), and thus doping only 20% Zn^{2+} did not change the property of the ZIF much. With an increase of zinc doping in $Co_{65}Zn_{35}$-ZIF (Figure 3C), although ATP still caused 56% fluorescence recovery, its response to GTP (approximately 83%) was higher.

Interestingly, when the content of cobalt and zinc was equal, $Co_{50}Zn_{50}$-ZIF exhibited a high fluorescence signal only in the presence of GTP (Figure 3D). Even though ATP, CTP and UTP have the same triphosphate unit as GTP, less than 20% of the DNA was desorbed with them. Figure 3A shows a fluorescence image of the free FAM-12mer. After $Co_{50}Zn_{50}$-ZIF was added, the fluorescence was completely quenched. The fluorescence was fully recovered after adding 2 mM GTP. Since guanosine and STPP alone induced nearly no DNA desorption at all, $Co_{50}Zn_{50}$-ZIF specifically recognized GTP due to its nucleobase and triphosphate being in the same molecule. The kinetics of fluorescence increase from $Co_{50}Zn_{50}$-ZIF further confirmed its excellent selectivity for GTP (Figure 3E).

When the content of zinc was further increased to 80%, the selectivity to GTP was decreased, and FAM-12mer/$Co_{20}Zn_{80}$-ZIF showed obvious signal to all the four nucleoside triphosphates (Figure 3F), which behaved similar to ZIF-8 (Zn) [30]. More DNA desorbed from $Co_{20}Zn_{80}$-ZIF with longer phosphate chains, indicating the critical role of the phosphate backbone in DNA for the adsorption. The kinetics of fluorescence increase supportive of DNA desorption

from $Co_{80}Zn_{20}$-ZIF, $Co_{65}Zn_{35}$-ZIF and $Co_{20}Zn_{80}$-ZIF are shown in Figure S2, and most systems reached saturated signal in 20 min. Overall, $Co_{50}Zn_{50}$-ZIF exhibited excellent selectivity for GTP.

Finally, we employed bovine serum albumin (BSA) and 12-mer random DNA (rDNA) as competitors to test the stability of the adsorbed DNA (Figure 3). Neither of them could detach the FAM-12mer from the surface of the four CoZn-ZIFs, suggesting that these CoZn-ZIFs can resist interference from biopolymers and are potentially useful in biological sample matrix.

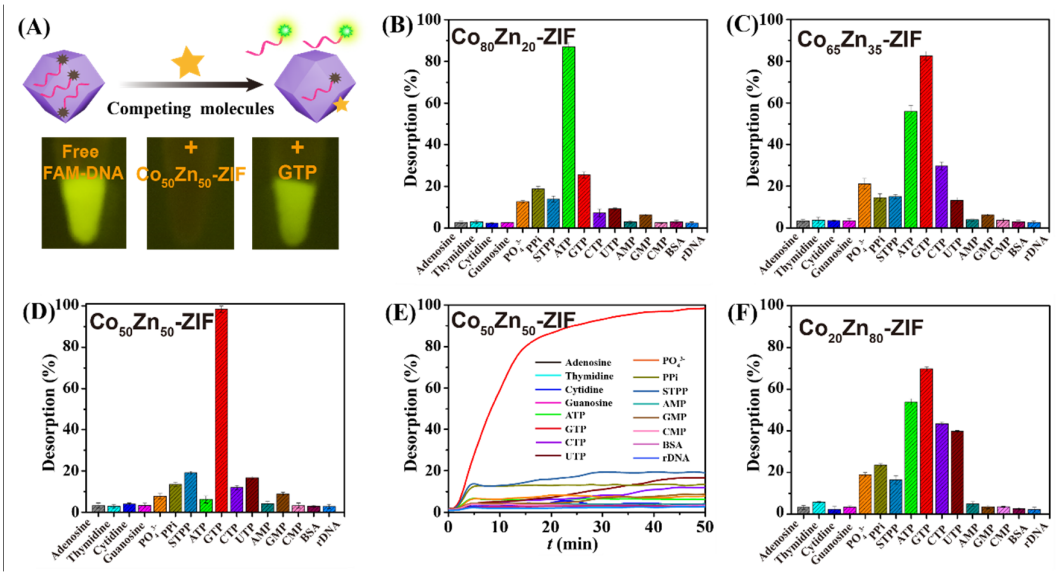


Figure 3. (A) DNA displacement by competing molecules, and fluorescence photographs of free FAM-12mer (100 nM), after adding $Co_{50}Zn_{50}$-ZIF (200 μg/mL), and after adding GTP (2 mM). Desorption percentages of FAM-12mer (10 nM) from 100 μg/mL of (B) $Co_{80}Zn_{20}$-ZIF, (C) $Co_{65}Zn_{35}$-ZIF, (D) $Co_{50}Zn_{50}$-ZIF and (F) $Co_{20}Zn_{80}$-ZIF induced by 1 mM different competing agents after 55 min of incubation. (E) The corresponding desorption kinetics of FAM-12mer from $Co_{50}Zn_{50}$-ZIF upon adding 1 mM competing molecules, 100 μg/mL BSA or 100 nM rDNA. Each measurement was repeated three times in HEPES buffer (10 mM, pH 7.6).

3.3 Both Co^{2+} and Zn^{2+} in $Co_{50}Zn_{50}$-ZIF are important for recognizing GTP

To further understand the mechanism of the specific GTP recognition by $Co_{50}Zn_{50}$-ZIF, other Co-based bimetallic ZIFs were also compared. We tried to prepare $Co_{50}Ni_{50}$-ZIF and $Co_{50}Cu_{50}$-ZIF using the same synthesis protocol as Figure 1A. However, ICP-MS analysis showed that the actual molar ratios of Ni and Cu were only 1.2% and 8.3% for $Co_{50}Ni_{50}$-ZIF and $Co_{50}Cu_{50}$-ZIF, respectively, much lower than the initial percentage added during the synthesis (50%). Although the morphologies of $Co_{50}Ni_{50}$-ZIF and $Co_{50}Cu_{50}$-ZIF were similar

to that of $Co_{50}Zn_{50}$-ZIF (Figure S3A and Figure S3B), they were very different in particle size, especially $Co_{50}Cu_{50}$-ZIF exhibited a very large size of ~4 μm. The ZIF structures of $Co_{50}Ni_{50}$-ZIF and $Co_{50}Cu_{50}$-ZIF were confirmed by PXRD (Figure S3C). Both materials had a positive surface charge as well (Figure S3D).

We then adsorbed the FAM-12mer to these two new ZIFs and added the competing molecules (Figure S4). FAM-12mer desorption from $Co_{50}Ni_{50}$-ZIF occurred most with GTP and CTP (80%), followed by UTP (65%) and ATP (53%). For $Co_{50}Cu_{50}$-ZIF, the NTPs showed a similar desorption efficiency at 70%, except that ATP was slightly lower (60%). Therefore, neither $Co_{50}Ni_{50}$-ZIF nor $Co_{50}Cu_{50}$-ZIF was selective to any of the molecules. Therefore, a synergetic effect of cobalt and zinc in $Co_{50}Zn_{50}$-ZIF was important for the excellent recognition of GTP. It is likely that the triphosphate and the guanine base were interacting with these two types of metals in a cooperative manner to yield such a highly specific recognition.

3.4 Highly sensitive detection of GTP

Inspired by the selective recognition of GTP by $Co_{50}Zn_{50}$-ZIF, we constructed a fluorescent assay for GTP detection (Figure 4A). The sensitivity of the sensor was tested by adding different concentrations of GTP, and more GTP induced a faster increase of the fluorescence (Figure 4B). The fluorescence enhancement (F/F_0-1) at 55 min was plotted as a function of GTP concentration (Figure 4C), and a linear response was observed with a detection limit of 0.13 μM GTP based on 3σ/slope (σ is the standard deviation of the background fluorescence in the absence of GTP), demonstrating a high sensitivity of the as-fabricated fluorescent biosensor. This sensitivity compared favorably with other biosensors for the detection of GTP (Table S1).

Moreover, the practicality of the proposed GTP biosensor was further evaluated in 1% fetal bovine serum (FBS). As shown in Figure 4D and Figure 4E, the fluorescence enhancement of FAM-12mer increased gradually with increasing GTP concentration. In addition, as shown in Table S2, the recovery rates are in the range of 81.8-111.2%, while the *RSD* is from 1.9% to 4.2%, indicating the potential of this assay for GTP determination in complex sample matrix.

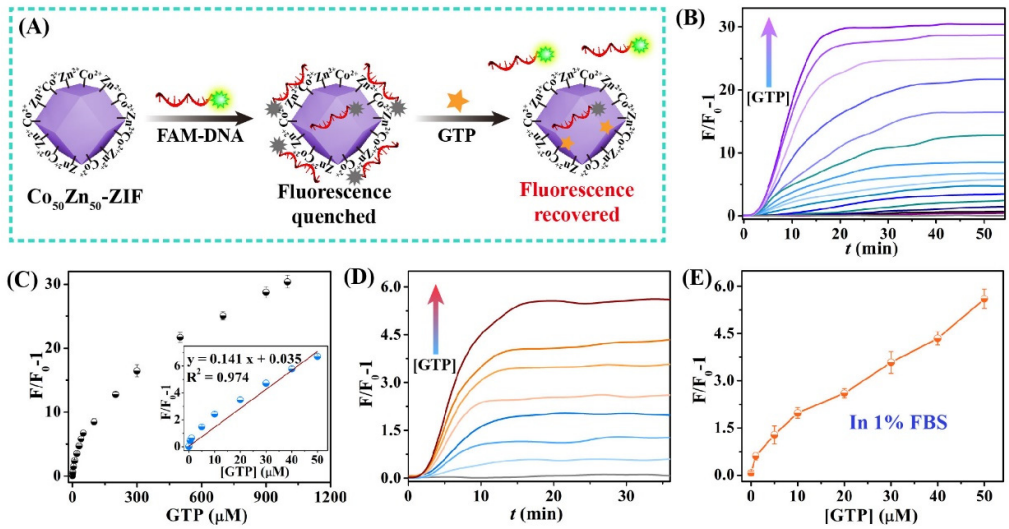


Figure 4. (A) Schematic illustration of fluorescence sensing of GTP on the basis of DNA desorption from $Co_{50}Zn_{50}$-ZIF. (B) Kinetics of sensor fluorescent recovery and (C) relative fluorescence enhancement of FAM-12mer DNA (10 nM) from 100 μg/mL $Co_{50}Zn_{50}$-ZIF induced by different concentrations of GTP. Inset: a linearity fitted relationship in the low concentration range. (D) Kinetics of fluorescent recovery and (E) relative fluorescence enhancement of FAM-12mer desorbed from $Co_{50}Zn_{50}$-ZIF induced by varying concentrations of GTP in 1% FBS. Each measurement was run in triplicate.

3.5 Discrimination of NTPs by a CoZn-ZIF sensor array

Since different NTPs have distinct responses in terms of fluorescence recovery from the four DNA/CoZn-ZIFs, we reason a fluorescent sensor array incorporating all these ZIFs might be useful for the discrimination of all the four NTPs (Figure 5A) [50]. To evaluate the discrimination capability of the sensor array, FAM-12mer was first respectively adsorbed on $Co_{80}Zn_{20}$-ZIF, $Co_{65}Zn_{35}$-ZIF, $Co_{50}Zn_{50}$-ZIF and $Co_{20}Zn_{80}$-ZIF, and then the DNA fluorescence recovery induced by ATP, GTP, CTP and UTP was respectively recorded. As shown in Figure 5B, 50 μM NTPs exhibited differential patterns on the fluorescence responses.

Principal component analysis (PCA) was then performed based on the fluorescence patterns of the training matrix (4 ZIFs × 4 NTPs × 6 replicates) to obtain a 2D canonical plot [51]. As can be seen in Figure 5C, the canonical patterns were divided into four groups, in which all four NTPs were well separated from each other without misclassification. The first two most significant discrimination factors PC1 and PC2 accounts for 68.3% and 30.9% of the total variability in the data respectively. From the hierarchical cluster analysis (HCA) mode (Figure 5D), the four different NTPs could also be clearly separated without being cross-affected by the ZIF sensor array.

In addition, to evaluate the quantitative ability of the ZIF sensor array, discrimination assays were performed for different concentrations of GTP as a model analyte, which could be clearly distinguished in the PCA (Figure 5E).

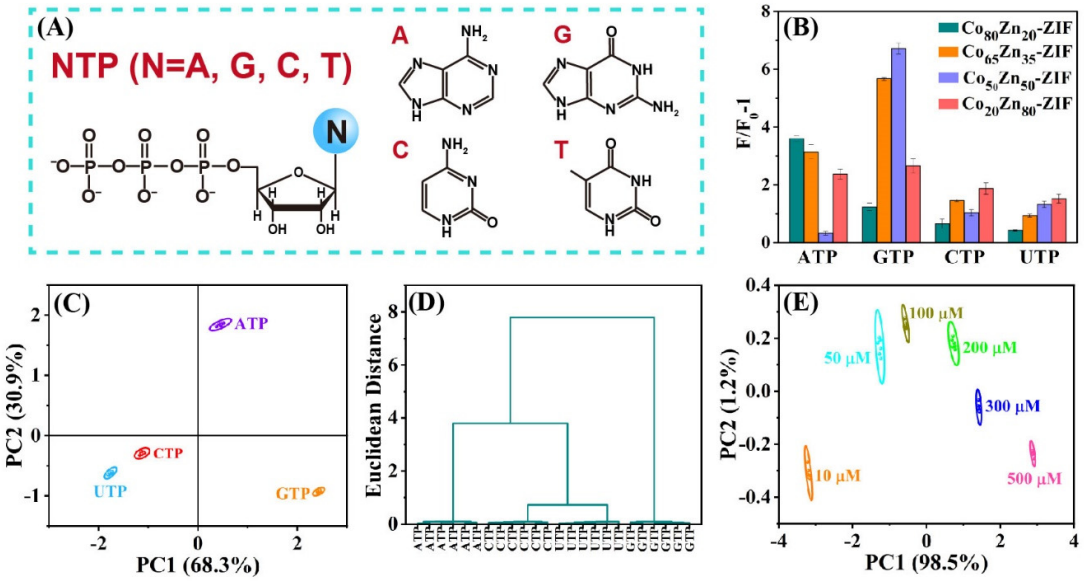


Figure 5. (A) Structures of various nucleobases and NTPs. (B) Relative fluorescence enhancement of FAM-12mer (10 nM) from the four CoZn-ZIFs induced by different NTPs (50 μM). (C) PCA and (D) HCA plot for the discrimination of the four NTPs. (E) PCA of the CoZn-ZIF sensor array for the identification of different concentrations of GTP. Each error bar was calculated from six independent measurements, and the ellipses indicate 95% confidence level.

4. Conclusions

In summary, we synthesized a series of homobimetallic Co_xZn_{100-x}-ZIF (x=0, 20, 50, 65, 80, 100) by tuning the contents of Co and Zn, and the actual molar percentages of Co were 0.03, 26.3, 55.7, 66.8, 84.1 and 99.6, respectively. In addition, the interaction between the CoZn-ZIFs and various phosphate-containing molecules was investigated using a fluorescently-labeled DNA as a probe. We discovered that GTP can readily displace adsorbed DNA from $Co_{50}Zn_{50}$-ZIF, and showed up to 30-fold fluorescence enhancement with 1 mM GTP. $Co_{80}Zn_{20}$-ZIF could specifically recognize ATP, whereas $Co_{65}Zn_{35}$-ZIF and $Co_{20}Zn_{80}$-ZIF responded to both. Based on the varying binding affinities of these CoZn-ZIFs towards different phosphate-containing analytes, we not only developed a highly sensitive sensor for GTP with a detection limit of 0.13 μM, but also designed a ZIF fluorescent sensor array for the discrimination of four types of NTPs. This system was also performed in a biological sample matrix and showed excellent practicality.

CRediT authorship contribution statement

Zhen Wang: Methodology, Data curation, Software, Writing – original draft. **Xumei Zhou:** Software and Data curation. **Jing Han:** Investigation and Methodology. **Gang Xie:** Supervision and Validation. **Juewen Liu:** Conceptualization, Writing – review & editing, Funding acquisition, Supervision. All authors approved the final version for publication.

Declaration of Competing Interest

The authors declare that they have no known competing financial interests or personal relationships that could have appeared to influence the work reported in this paper.

Acknowledgments

Funding for this work was from the Natural Sciences and Engineering Research Council of Canada (NSERC). Z. Wang was supported by a China Scholarship Council Scholarship to visit the University of Waterloo.

References

[1] H.R. Bourne, D.A. Sanders, F. McCormick, The GTPase superfamily: a conserved switch for diverse cell functions, Nature 348 (1990) 125−132.

[2] S. Nakano, M. Fukuda, T. Tamura, R. Sakaguchi, E. Nakata, T. Morii, Simultaneous detection of ATP and GTP by covalently linked fluorescent ribonucleopeptide sensors, J. Am. Chem. Soc. 135 (2013) 3465−3473.

[3] Y. Li, J. Liu, Sensing guanine and its derivatives: from molecular recognition to applications, Sensors and Actuators Reports 2 (2020) 100020.

[4] B. Alberts, A. Johnson, J. Lewis, M. Raff, K. Roberts, P. Walter, Molecular biology of the cell, 4th ed, Wiley: New York, 2002.

[5] F. Janiak, V.A. Dell, J.K. Abrahamson, B.S. Watson, D.L. Miller, A.E. Johnson, Fluorescence characterization of the interaction of various transfer RNA species with elongation factor Tu·GTP: evidence for a new functional role for elongation factor Tu in protein biosynthesis, Biochemistry 29 (1990) 4268−4277.

[6] N.B.V. Sepuri, N. Schülke, D. Pain, GTP hydrolysis is essential for protein import into the mitochondrial matrix, J. Biol. Chem. 273 (1998) 1420−1424.

[7] J. Downward, Targeting RAS signalling pathways in cancer therapy, Nat. Rev. Cancer 3 (2003) 11−22.

[8] P. Jagodzinski, S. Lizakowski, R.T. Smolenski, E.M. Slominska, D. Goldsmith, H.A. Simmonds, B. Rutkowski, Mycophenolate mofetil treatment following renal transplantation decreases GTP concentrations in mononuclear leucocytes, Clin. Sci. 107 (2004) 69−74.

[9] I. Rubio, R. Pusch, R. Wetzker, Quantification of absolute Ras-GDP/GTP levels by HPLC separation of Ras-bound [^{32}P]-labelled nucleotides, J. Biochem. Bioph. Meth. 58 (2004) 111−117.

[10] C. Bolin, F. Cardozo-Pelaez, Assessing biomarkers of oxidative stress: analysis of guanosine and oxidized guanosine nucleotide triphosphates by high performance liquid chromatography with electrochemical detection, J. Chromatogr. B 856 (2007) 121−130.

[11] M. Huang, Y. Wang, Global and targeted profiling of GTP-binding proteins in biological samples by mass spectrometry, Mass Spectrom. Rev. 40 (2021) 215−235.

[12] R.N. Goyal, M. Oyama, A. Tyagi, Simultaneous determination of guanosine and guanosine-5′-triphosphate in biological sample using gold nanoparticles modified indium tin oxide electrode, Anal. Chim. Acta 581 (2007) 32−36.

[13] N.J. Wu, J.B. Lan, L.P. Yan, J.S. You, A sensitive colorimetric and fluorescent sensor based on imidazolium-functionalized squaraines for the detection of GTP and alkaline phosphatase in aqueous solution, Chem. Commun. 50 (2014) 4438−4441.

[14] E.A. Weitz, J.Y. Chang, A.H. Rosenfield, E.A. Morrow, V.C. Pierre, The basis for the molecular recognition and the selective time-gated luminescence detection of ATP and GTP by a lanthanide complex, Chem. Sci. 4 (2013) 4052−4060.

[15] P.P. Neelakandan, M. Hariharan, D. Ramaiah, A supramolecular ON-OFF-ON fluorescence assay for selective recognition of GTP, J. Am. Chem. Soc. 128 (2006) 11334−11335.

[16] S. Wang, Y.-T. Chang, Combinatorial synthesis of benzimidazolium dyes and its diversity directed application toward GTPselective fluorescent chemosensors, J. Am. Chem. Soc. 128 (2006) 10380−10381.

[17] J.Y. Kwon, N.J. Singh, H.N. Kim, S.K. Kim, K.S. Kim, J. Yoon, Fluorescent GTP-sensing in aqueous solution of physiological pH, J. Am. Chem. Soc. 126 (2004) 8892−8893.

[18] M.L. Aulsebrook, M. Starck, M.R. Grace, B. Graham, P. Thordarson, R. Pal, K.L. Tuck, Interaction of nucleotides with a trinuclear terbium (III)-dizinc (II) complex: efficient sensitization of terbium luminescence by guanosine monophosphate and application to real-time monitoring of phosphodiesterase activity, Inorg. Chem. 58 (2019) 495−505.

[19] L.S. Mittal, P. Sharma, N. Kaur, P. Singh, A perylenediimide based 'on-off'chemosensor for the detection of nucleoside triphosphates: an efficient ensemble for monitoring alkaline phosphatase activity, Anal. Methods 11 (2019) 5320−5327.

[20] I.J. Bazany-Rodríguez, M.K. Salomón-Flores, J.M. Bautista-Renedo, N. González-Rivas, A. Dorazco-González, Chemosensing of guanosine triphosphate based on a fluorescent dinuclear Zn (II)-dipicolylamine complex in water, Inorg. Chem. 59 (2020) 7739−7751.

[21] B. Liu, Z. Sun, P.J.J. Huang, J. Liu, Hydrogen peroxide displacing DNA from nanoceria: mechanism and detection of glucose in serum, J. Am. Chem. Soc. 137 (2015) 1290−1295.

[22] H. Furukawa, K.E. Cordova, M. O'Keeffe, O.M. Yaghi, The chemistry and applications of metal-organic frameworks, Science 341 (2013) 1230444.

[23] Y. Zhao, H. Zeng, X.W. Zhu, W. Lu, D. Li, Metal-organic frameworks as photoluminescent biosensing platforms: mechanisms and applications, Chem. Soc. Rev. 50 (2021) 4484−4513.

[24] N.B. Shustova, A.F. Cozzolino, S. Reineke, M. Baldo, M. Dincă, Selective turn-on ammonia sensing enabled by high-temperature fluorescence in metal-organic frameworks with open metal sites, J. Am. Chem. Soc. 135 (2013) 13326−13329.

[25] X.L. Yang, C. Ding, R.F. Guan, W.H. Zhang, Y. Feng, M.H. Xie, Selective dual detection of H_2S and Cu^{2+} by a post-modified MOF sensor following a tandem process, J. Hazard. Mater. 403 (2021) 123698.

[26] X. Qian, S. Deng, X. Chen, Q. Gao, Y.L. Hou, A. Wang, L. Chen, A highly stable, luminescent and layered zinc (II)-MOF: Iron (III)/copper (II) dual sensing and guest-assisted exfoliation, Chinese Chem. Lett. 31 (2020) 2211−2214.

[27] L. Guo, M. Wang, D. Cao, A novel Zr-MOF as fluorescence turn-on probe for real-time detecting H_2S gas and fingerprint identification, Small 14 (2018) 1703822.

[28] R. Xu; Y. Wang, X. Duan, K. Lu, D. Micheroni, A. Hu, W. Lin, Nanoscale metal-organic frameworks for ratiometric oxygen sensing in live cells, J. Am. Chem. Soc. 138 (2016) 2158−2161.

[29] P. Kumar, K.H. Kim, S. Rarotra, L. Ge, G. Lisak, The advanced sensing systems for NOx based on metal-organic frameworks: applications and future opportunities, Trac-Trend. Anal. Chem. 122 (2020) 115730.

[30] Z. Wang, X. Zhou, Y. Li, Z. Huang, J. Han, G. Xie, J. Liu, Sensing ATP: zeolitic imidazolate framework-67 is superior to aptamers for target recognition, Anal. Chem. 93 (2021) 7707−7713.

[31] X. Shi, H. Xu, Y. Wu, Y. Zhao, H.M. Meng, Z. Li, L. Qu, Two-dimension (2D) Cu-MOFs/aptamer nanoprobe for in situ ATP imaging in living cells, J. Anal. Test. 5 (2021) 165−173.

[32] M.Y. Masoomi, A. Morsali, A. Dhakshinamoorthy, H. Garcia, Mixed-metal MOFs: unique opportunities in metal-organic framework (MOF) functionality and design, Angew. Chem., Int. Ed. 131 (2019) 15330−15347.

[33] Y. Ban, Y. Li, Y. Peng, H. Jin, W. Jiao, X. Liu, W. Yang, Metal-substituted zeolitic imidazolate framework ZIF-108: gas-sorption and membrane-separation properties, Chem. Eur. J. 20 (2014) 11402−11409.

[34] Z. Wang, X. Zhou, Z. Huang, J. Han, G. Xie, J. Liu, A sensor array based on DNA-wrapped bimetallic zeolitic imidazolate frameworks for detection of ATP hydrolysis products, Nanoscale 14 (2022) 26−34.

[35] Y. Zhou, T. Yang, R. Namivandi-Zangeneh, C. Boyer, K. Liang, R. Chandrawati, Copper-doped metal-organic frameworks for the controlled generation of nitric oxide from endogenous S-nitrosothiols, J. Mater. Chem. B 9 (2021) 1059−1068.

[36] H. Yang, X.W. He, F. Wang, Y. Kang, J. Zhang, Doping copper into ZIF-67 for enhancing gas uptake capacity and visible-light-driven photocatalytic degradation of organic dye, J. Mater. Chem. 22 (2012) 21849−21851.

[37] A. Schejn, A. Aboulaich, L. Balan, V. Falk, J. Lalevée, G. Medjahdi, L. Aranda, K. Mozet, R. Schneider, Cu^{2+}-doped zeolitic imidazolate frameworks (ZIF-8): efficient and stable catalysts for cycloadditions and condensation reactions, Catal. Sci. Technol. 5 (2015) 1829−1839.

[38] G. Kaur, R.K. Rai, D. Tyagi, X. Yao, P.Z. Li, X.C. Yang, Y.L. Zhao, Q. Xu, S.K. Singh, Room-temperature synthesis of bimetallic Co-Zn based zeolitic imidazolate frameworks in water for enhanced CO_2 and H_2 uptakes, J. Mater. Chem. A 4 (2016) 14932−14938.

[39] K. Zhou, B. Mousavi, Z. Luo, S. Phatanasri, S. Chaemchuen, F. Verpoort, Characterization and properties of Zn/Co zeolitic imidazolate frameworks vs. ZIF-8 and ZIF-67, J. Mater. Chem. A 5 (2017) 952−957.

[40] S. Lai, L. Xu, H. Liu, S. Chen, R. Cai, L. Zhang, W. Theis, J. Sun, D. Yang, X. Zhao, Controllable synthesis of CoN_3 catalysts derived from Co/Zn-ZIF-67 for electrocatalytic oxygen reduction in acidic electrolytes, J. Mater. Chem. A 7 (2019) 21884−21891.

[41] Y.Z. Chen, C. Wang, Z.Y. Wu, Y. Xiong, Q. Xu, S.H. Yu, H.L. Jiang, From bimetallic metal-organic framework to porous carbon: high surface area and multicomponent active dopants for excellent electrocatalysis, Adv. Mater. 27 (2015) 5010−5016.

[42] J. Yang, F. Zhang, H. Lu, X. Hong, H. Jiang, Y. Wu, Y. Li, Hollow Zn/Co ZIF particles derived from core-shell ZIF-67@ZIF-8 as selective catalyst for the semi-hydrogenation of acetylene, Angew. Chem., Int. Ed. 127 (2015) 11039−11043.

[43] S. Li, Y. Hou, Q. Chen, X. Zhang, H. Cao, Y. Huang, Promoting active sites in MOF-derived homobimetallic hollow nanocages as a high-performance multifunctional nanozyme catalyst for biosensing and organic pollutant degradation, ACS Appl. Mater. Interfaces 12 (2019) 2581−2590.

[44] H. Hayashi, A.P. Cote, H. Furukawa, M. O'Keeffe, O.M. Yaghi, Zeolite A imidazolate frameworks, Nat.

Mater. 6 (2007) 501−506.

[45] A.F. Gross, E. Sherman, J.J. Vajo, Aqueous room temperature synthesis of cobalt and zinc sodalite zeolitic imidizolate frameworks, Dalton Trans. 41 (2012) 5458−5460.

[46] R. Li, X. Ren, H. Ma, X. Feng, Z. Lin, X. Li, C. Hu, B. Wang, Nickel-substituted zeolitic imidazolate frameworks for time-resolved alcohol sensing and photocatalysis under visible light, J. Mater. Chem. A 2 (2014) 5724−5729.

[47] M.P. Kushalkar, B. Liu, J. Liu, Promoting DNA adsorption by acids and polyvalent cations: beyond charge screening, Langmuir 36 (2020) 11183−11195.

[48] A. Lopez, Y. Zhao, Z. Huang, Y. Guo, S. Guan, Y. Jia, J. Liu, Poly-cytosine deoxyribonucleic acid strongly anchoring on graphene oxide due to flexible backbone phosphate interactions, Adv. Mater. Interfaces 8 (2021) 2001798.

[49] Z. Wang, Z. Huang, J. Han, G. Xie, J. Liu, Polyvalent metal ion promoted adsorption of DNA oligonucleotides by montmorillonite, Langmuir 37 (2021) 1037−1044.

[50] Z.H. Chen, Q.X. Fan, X.Y. Han, G. Shi, M. Zhang, Design of smart chemical ‘tongue’sensor arrays for pattern-recognition-based biochemical sensing applications, Trac-Trend. Anal. Chem. 124 (2020) 115794.

[51] I.T. Jolliffe, J. Cadima, Principal component analysis: a review and recent developments, Philos. T. R. Soc. A 374 (2016) 20150202.